Field-Induced Modulated State in the Ferromagnet PrPtAl

Christopher D. O'Neill,[1,*] Gino Abdul-Jabbar,[1] Didier Wermeille,[2] Philippe Bourges,[3] Frank Krüger,[4,5] and Andrew D. Huxley[1]

[1]School of Physics and CSEC, University of Edinburgh, Edinburgh EH9 3FD, United Kingdom
[2]XMAS, ESRF, BP220, F-38043 Grenoble, France
[3]Laboratoire Léon Brillouin (UMR12 CEA-CNRS), 91191 Gif-sur-Yvette Cedex, France
[4]London Centre for Nanotechnology, University College London, Gordon Street, London WC1H 0AH, United Kingdom
[5]ISIS Facility, Rutherford Appleton Laboratory, Chilton, Didcot, Oxfordshire OX11 0QX, United Kingdom

(Received 2 September 2020; accepted 13 April 2021; published 13 May 2021)

The theory of quantum order-by-disorder (QOBD) explains the formation of modulated magnetic states at the boundary between ferromagnetism and paramagnetism in zero field. PrPtAl has been argued to provide an archetype for this. Here, we report the phase diagram in magnetic field, applied along both the easy a axis and hard b axis. For field aligned to the b axis, we find that the magnetic transition temperatures are suppressed and at low temperature there is a single modulated fan state, separating an easy a axis ferromagnetic state from a field polarized state. This fan state is well explained with the QOBD theory in the presence of anisotropy and field. Experimental evidence supporting the QOBD explanation is provided by the large increase in the T^2 coefficient of the resistivity and direct detection of enhanced magnetic fluctuations with inelastic neutron scattering, across the field range spanned by the fan state. This shows that the QOBD mechanism can explain field induced modulated states that persist to very low temperature.

DOI: 10.1103/PhysRevLett.126.197203

The suppression of magnetic order by pressure (P) or chemical substitution is a proven approach to discover new quantum phases of matter, such as unconventional superconductivity. In clean metallic antiferromagnets, the transition remains continuous as the ordering temperature is suppressed by the tuning parameter, resulting in a quantum critical point (QCP) at zero temperature. For clean metallic ferromagnets a QCP is, however, avoided in one of two ways [1]. In the first, the transition becomes 1st order at a tricritical point (TCP). Tuning beyond this point, metamagnetic transitions occur at finite field along the easy axis that give rise to wings in the P-H-T phase diagram, across which the uniform moment is discontinuous (H is the magnetic field). This mechanism arises from coupling to any bosonic mode at zero wave vector [2–4]. Examples include UGe_2 [5,6] and $ZrZn_2$ [7]. In the second way a modulated state is formed between the ferromagnetic (FM) and paramagnetic (PM) states [8,9]. This is driven by increased particle-hole fluctuations around the deformed Fermi surface in the modulated state, a mechanism known as quantum order by disorder (QOBD) [10].

The first reported observation of such a modulated state was in PrPtAl [11], but those measurements did not access the QCP. A modulated state was later observed in the itinerant magnet $Nb_{1-y}Fe_{2+y}$ [12,13], at low temperature for $y \approx 0$ between two FM states, with $y \gtrsim 0.004$ and $y \lesssim -0.012$ [12]. For excess Fe ($y \gtrsim 0.004$), the modulated state is undercut by FM at low temperature, giving a behavior resembling that in PrPtAl. An avoided QCP under pressure in $LaCrGe_3$ [14,15] has recently been shown to give way to short-range order, rather than long-range modulated antiferromagnetism [16].

For PrPtAl, neutron and resonant x-ray scattering identified that as a function of temperature the PM to FM transition passes through two incommensurately modulated spin density wave states, SDW1 and SDW2. The SDW2 state fits well with predictions for QOBD [11]. However, there are some problems describing SDW1 in terms of QOBD, that we address in the present study. For SDW1 and SDW2, pressure does not suppress the ordering temperature, but enhances it, so the quantum regime where the transitions occur at very low, and ultimately zero temperature, has not so far been explored. Here, we show that a field transverse to the easy axis can provide an appropriate tuning parameter to depress the transition temperatures (to zero) in PrPtAl, giving a fan state (SDW3), that we explain with the QOBD theory in an applied field. This vastly expands the scope over which this theory has been successfully applied to include states that extend to zero temperature, compared with SDW1 and SDW2, which are confined to finite temperatures.

One of the most remarkable properties of the QOBD theory is that it explains order along magnetic hard axes [1]. In zero field this is manifest by states SDW1 and SDW2 with modulated moments (m) along both the a-axis (easy-axis) and b-axis (hard-axis) directions. The SDW3 state links the uniform states, FM and polarized PM, with different moment orientations. This provides an ideal

setting for the QOBD mechanism since the difference in energy between $m\|\mathbf{a}$ and $m\|\mathbf{b}$ is low in this region.

Mechanisms for forming SDW1 and SDW2, based on domain walls, a Devil's staircase generated by competing interactions, or an electronic nesting instability, have been ruled out in the previous work [11]. To treat PrPtAl the QOBD model for an itinerant system [9] was extended by the inclusion of local moments and anisotropy [11].

The magnetoresistance (MR) for field along the easy a axis is strongly negative in the SDW2 state with a cusplike maximum at $B = 0$, suggesting stronger fluctuations are present in the SDW2 state than in the FM state, supporting a QOBD based explanation for SDW2 (Supplemental Material, Fig. S2 [17]). The MR for SDW1, however, has a peak at low field which seems at odds with the expectation of the QOBD theory, assuming field suppresses the modulated order.

Here, we show that the amplitude of the SDW1 state is in fact initially enhanced with magnetic field before being suppressed at higher field. The increase of the MR is then perfectly consistent with QOBD. This is because in a QOBD state the fluctuations are enhanced along with the amplitude of the order. In contrast, for non-QOBD states magnetic fluctuations are peaked at a phase transition, but are suppressed entering the ordered state. The correlation we report between the order and MR, therefore, provides clear evidence that both SDW1 and SDW2 are explained by the QOBD mechanism.

A comprehensive description of the sample and experimental methods is given in the Supplemental Material [17]. Resonant x-ray scattering intensity from high quality single crystals of PrPtAl, for fields along the b and a axis, is shown in Fig. 1 and Fig. 2, respectively. Measurements were carried out at the 6.444 keV Pr L_2 edge (this energy gives access to several Brillouin zones and avoids the surface sensitivity at lower energy M_4 and M_5 edges). These measurements are sensitive to magnetic moments directed along **a**. We discuss first the low field (< 50 mT) measurements for both axes, and then higher field measurements for $H\|\mathbf{b}$. The overall phase diagram is shown in Fig. 4. As found previously in zero field, SDW1 exists below $T_1 = 5.85 \pm 0.05$ K with $q_1 \approx (0, 0, 0.10)$, accompanied by a second state with a modulation vector, that we label here, $q_4 \approx (0, 0, 0.235)$. Below $T_2 = 5.45 \pm 0.35$ K, these states are replaced by SDW2 with $q_2 \approx (0, 0, 0.07)$ and a third harmonic. We find that the modulation at q_4 is suppressed by residual fields in our magnets. Thus, the q_4 intensity seen in the inset of Fig. 2(a) (no magnet) is not present in Fig. 2(d). Figure 2(c) shows that for $H\|\mathbf{a}$, the intensity of the q_1 modulation of SDW1 is initially

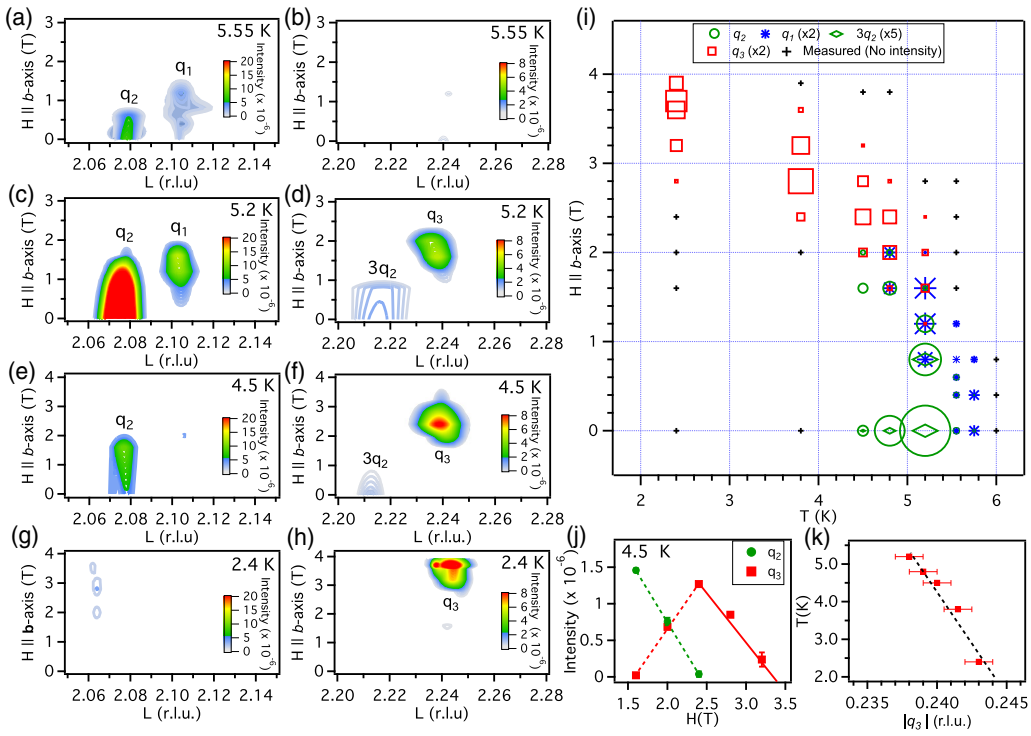

FIG. 1. Color-scale images of normalized magnetic resonant x-ray scattered intensity as a function of field (H) applied along the b axis and scattering vector $(0, 0, L)$ at (a) and (b) 5.55, (c) and (d) 5.2, (e) and (f) 4.5, and (g) and (h) 2.4 K. Scattering at wave vectors q_1 and q_2 survives up to 2 T, before abruptly being replaced by scattering at wave vector q_3. (i) The $H - T$ phase diagram showing the integrated intensity at q_1, q_2, q_3, and $3q_2$ up to 4 T. The marker size is proportional to the integrated intensity (scaling shown in the legend). Measured points where no intensity was found are marked by crosses. (j) The variation in integrated intensity at q_2 and q_3 with H at 4.5 K. (k) T dependence of the magnitude of q_3 (the dashed line is a guide to the eye).

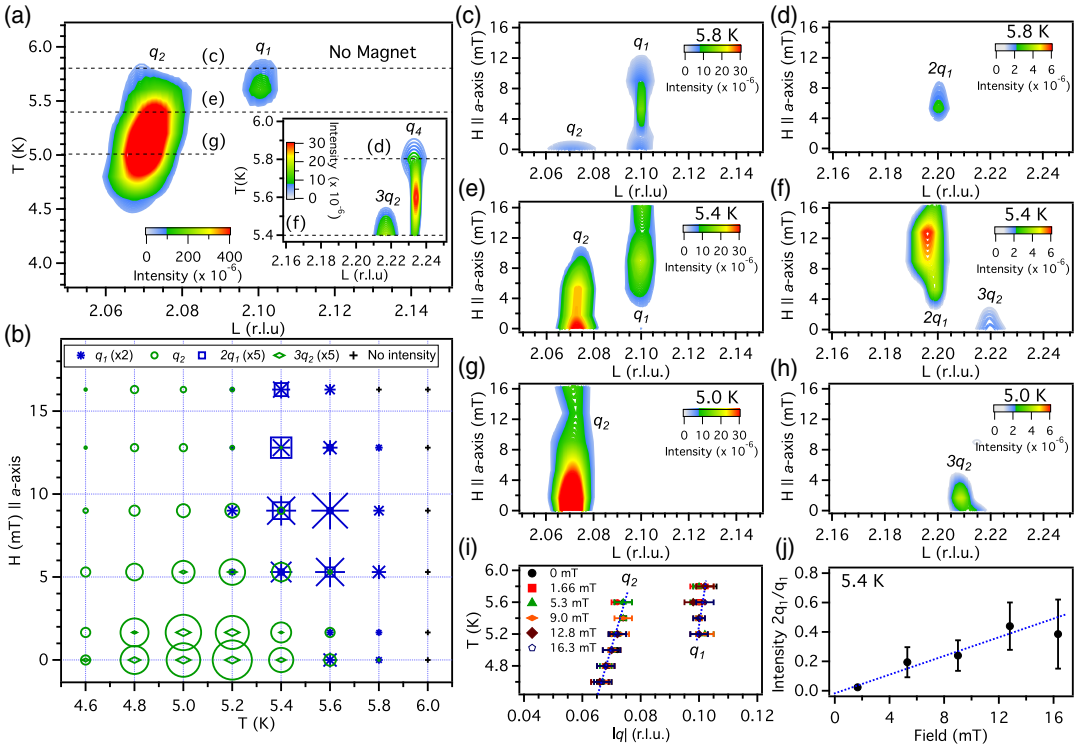

FIG. 2. (a) Color-scale image of the normalized magnetic resonant x-ray scattered intensity as a function of T and reciprocal lattice coordinate $(0, 0, L)$ in zero field (no magnet). Inset, the corresponding intensity at wave vectors q_4 and $3q_2$. (b) $H - T$ phase diagram of the integrated intensity at q_1, q_2, $2q_1$, and $3q_2$ for H applied along the a axis. The marker size is proportional to the normalized integrated intensity (scaling is shown in the legend). Measured points where no intensity is found are marked by crosses. The data at zero field in this plot are with the magnet in place. (c)–(h) Color-scale maps of scattered intensity as a function of H along the a axis and $(0, 0, L)$ for 5.8, 5.4, and 5.0 K [the corresponding temperatures at zero field are marked by dashed lines in (a)]. (i) T dependence of q_1 and q_2. Points at different field superimpose. Dashed lines are guides to the eye showing that both q_1 and q_2 increase linearly with temperature. (j) The ratio of integrated intensity between the second harmonic $2q_1$ and q_1 at 5.4 K as a function of field. The dashed line is a guide to the eye.

enhanced, and is maximum at 10 mT, where it is accompanied by a second harmonic [Figs. 2(e) and 2(f)]. No $2q_1$ signal is induced for field $\|\mathbf{b}$. The MR for field along the a axis (Supplemental Material, Fig. S2 [17]), contains a small positive maximum at 10 mT in SDW1 that as explained above may now be understood to be a consequence of the enhanced order in small applied field (in line with QOBD). $|q_1|$ and $|q_2|$ increase with temperature as expected by the QOBD mechanism, shown in Fig. 2(i). No changes of q_1 and q_2 are seen with field.

We now discuss larger fields applied along the b axis (Fig. 1). SDW1 and SDW2 survive to ~2 T before switching to SDW3 with modulation vector $q_3 \approx 0.24$ [Figs. 1(c)–1(f)]. The magnitude of the critical field (2 T) is comparable to the conventional anisotropy field estimated in Ref. [11]. SDW3, then extends into the quantum regime at low temperature and high fields, which was the original target for the QOBD description. The integrated intensities of SDW2 and SDW3 as a function of field at 4.5 K, are shown in Fig. 1(j). At 1.6 T no SDW3 intensity is present, at 2 T it coexists with SDW2, replacing SDW2 entirely at 2.4 T consistent with a 1st order transition. Above 2.4 T, the intensity decreases continuously with field to zero above 3.2 T. The linear suppression of the intensity with field suggests that the high field transition is continuous. This is also confirmed with neutron scattering for $H\|b$ axis at 1.7 K (Supplemental Material, Fig. S1 [17]). The neutron scattering also confirms the uniform FM moment is suppressed when SDW3 appears (Supplemental Material, Fig. S1 [17]). The resolution limited SDW peaks and suppression of FM show that the SDW3 state is distinct from FM. SDW3 could be either a polarized spiral, a b-axis fan state, or an inclined plane wave state (these cannot be distinguished based on our data). A fan state, as found in field polarized rare earth helimagnets [23,24], might be considered the most likely choice, although the mechanism driving modulated state formation is quite different. Figure 1(k) shows that unlike q_1 and q_2, q_3 decreases with increasing temperature. Analogous to q_1 and q_2, no significant change of q_3 is seen with field.

MR for field along the b axis is shown in Fig. 3(a). Red markers show the transition fields seen with x rays. At the continuous transition to the fully polarized state, where the transverse magnetic susceptibility is expected to diverge, a

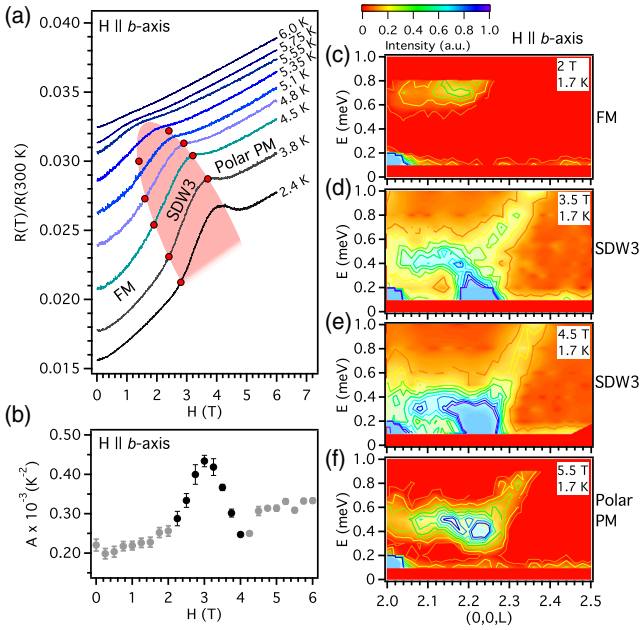

FIG. 3. (a) The MR, normalized to the zero field resistivity value at 300 K, for field applied along the b axis. The region where SDW3 exists is shaded red, with markers showing the transition field seen in x-ray scattering. (b) The A coefficient of resistivity for Fermi liquid fits between 4 and 2.2 K as a function of field. Black markers correspond to the region where SDW3 exists within this temperature range. (c)–(f) Color-scale images of inelastic neutron scattered intensity (in arbitrary units) as a function of energy transfer and reciprocal lattice coordinate $(0, 0, L)$ at 1.7 K for different fields applied along the b axis. These show the dispersion of the lowest energy magnetic excitation at (c) 2 T in the FM state, (d) 3.5 and (e) 4.5 T in the SDW3 state, and (f) 5.5 T in the polar PM state.

local maxima exists. The temperature range of the measurements does not permit a meaningful estimate of the power law describing the temperature dependence of the resistivity, however, the magnitude of the dependence can be estimated based on $\rho = \rho_0 + AT^2$. The A coefficient of resistivity as a function of field applied along the b axis is shown in Fig. 3(b), determined from the data between 2.2 and 4 K. In this temperature range, SDW3 exists between ~2 and 4.2 T. The temperature dependence of the resistivity is seen to be enhanced in the SDW3 state. The incommensurate modulation could provide an additional source of scattering. Following Matthiessen's rule, this would add an additional term to ρ_0. The magnitude of this term would depend on the amplitude and possibly the wave vector q_3 of the modulation. The SDW amplitude is suppressed with T, while q_3 changes only very modestly ($< 1\%$). Thus, the overall effect of such a contribution would be to decrease the total T dependence in the fan state (the opposite of what is seen). The increased T dependence observed, therefore, must reflect an increase in the DOS in SDW3 compared with FM and PM, which confirms a key prediction of the QOBD theory.

Inelastic neutron scattering spectra at 1.7 K, with $H\|\mathbf{b}$, are shown in Figs. 3(c)–3(f). For PrPtAl, there are 4 Pr atoms per unit cell and the crystalline electric field (CEF) environment splits the $4f^2$ Pr^{3+} ions into 9 nonmagnetic singlets. FM order is achieved by mixing singlets via an intersite exchange interaction [25,26]. At 2 T, in the FM state [Fig. 3(c)], scattering from the excitations of the lowest excited singlet exists between 0.6–0.8 meV, consistent with previous results in zero field [11]. In the SDW3 state, at 3.5 and 4.5 T (Fig. 3(d) and (e)), softening of this mode occurs at q_3. This softening, at nonzero q and the associated energy fluctuations, require long range interactions transmitted by the itinerant electrons. Conversely the interaction with the electrons results in strong damping of the CEF levels. The broad low energy intensity at 0–0.3 meV near q_3, is the direct observation of this. Enhanced scattering in the same energy range is also seen close to $q = 0$ (at (002)), which is a direct manifestation of an increased DOS [27]. Importantly, these strongly damped modes are also present at 3.5 T, well away from the critical field just above ~4.5 T, showing that strong electronic correlations are an intrinsic attribute of the incommensurate phase and are not limited to the critical field.

We now compare our results to the predictions of the QOBD model with magnetic anisotropy in an applied field. This model is described in detail in the Supplemental Material [17]. In PrPtAl, the local CEF environments are tilted in the $a - c$ plane. This means moments in the **a** direction also imply an implicit AF moment component along **c** within the unit cell. For simplicity, we omit mention of the c axis moments in the following. In previous QOBD calculations, only a helimagnet spiral state for SDW2 and uniform ferromagnetism were considered [11]. The order parameter for the moments in the helimagnet is

$$\mathbf{m}_{\text{helix}}(\mathbf{r}) = \begin{pmatrix} m_a \cos[qz + \phi(z)] \\ m_b \sin[qz + \phi(z) + \epsilon] \end{pmatrix} \tag{1}$$

with $\phi(z) = -\delta_{1a}\sin(qz) + \delta_{1b}\cos(qz) - \delta_2\sin(2qz)$, where q is the primary modulation vector, which is along z (c axis). Previously only $\delta_2 \neq 0$ was considered, which accounts for the deformation of the SDW2 state away from an evenly pitched spiral in response to the CEF and generates a third-order harmonic at $3q$ (Fig. 4, SDW2). The term ϵ switches between a spiral for $\epsilon = 0$ and an inclined plane wave for $\epsilon = \pm\pi/2$. This parameter has not been determined experimentally.

The $\delta_{1a,b}$ terms tilt moments towards a field along the a, b axis. These terms give a second-order harmonic. Experimentally the SDW2 state resists polarizing in a field (δ_1 terms small), whereas SDW1 polarizes strongly for $H\|\mathbf{a}$ [significant δ_{1a}, the relative intensity of the second harmonic against field is shown in Fig. 2(j)]. The lack of a 3rd-order harmonic for SDW1 indicates a weaker role of

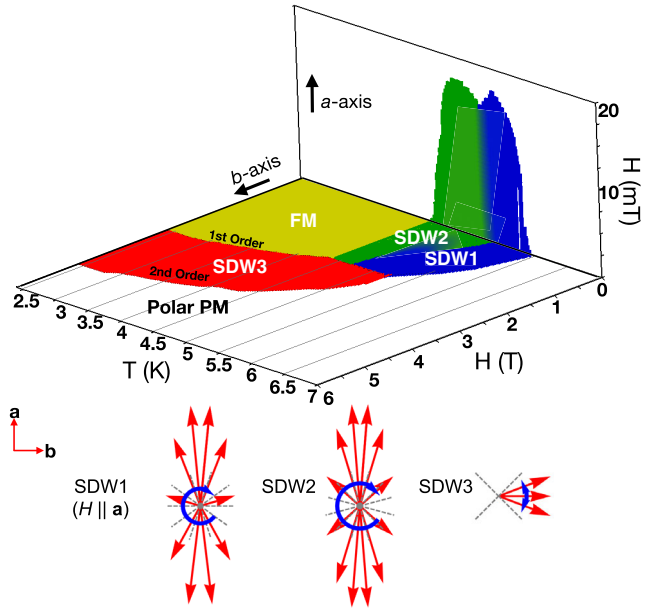

FIG. 4. The schematic H_a-H_b-T phase diagram for PrPtAl with fields applied along the easy a axis (vertical) and hard b axis (horizontal), based on our measurements. SDW1 (blue), SDW2 (green), and SDW3 (red) modulated states form a ridge around the first order FM plane (yellow) across which the FM moment $\mathbf{M}\|\mathbf{a}$ reverses. The phase boundaries between the different modulated states and on the low-field low-temperature side of the ridge are first order. Schematics of the moment directions viewed along the c axis for one modulation period for the different modulated states SDW1, SDW2, and SDW3 are shown below the phase diagram.

CEF anisotropy (δ_2 small) in this state compared with SDW2. Unequal moments along the a and b axes, i.e., $m_a \neq m_b$, provide another source of anisotropy, that does not result by itself in the generation of higher harmonic reflections. In polarized neutron scattering [11], it was found that the ratio of m_a to m_b was around 3 ± 0.5 at lower temperature where SDW2 predominates (for both the 1st and 3rd harmonics) and 2.5 ± 0.5 (for both SDW1 and SDW2) at higher temperatures. Thus, the intrinsic anisotropy m_a/m_b is similar in all the states.

In forming a modulated state, there is a loss of FM exchange energy since the moments are no longer locally aligned. This acts to minimize the modulation wave vector q. This is offset in the QOBD mechanism by the excess density of states created through modulation, roughly proportional to m^2q^2, which lowers the energy, favoring a large q. The optimum q results from a subtle balance of these two energies and is strongly dependent on temperature.

The crystal field anisotropy energy between the a and b axes is proportional to m^3 (or higher power of m) and also contributes to the energy balance [28,29]. It favors a state that has all the moments aligned in the preferred CEF direction (a axis). As the temperature increases, the magnitude of the ordered moment falls and the role of magnetic anisotropy decreases more rapidly than the other energy scales. This is consistent with the observed fall in the intensity of the third harmonic with temperature in the SDW2 state. For $H\|\mathbf{a}$, the polarizibility should grow with temperature as moments are less confined to the a axis. This is exactly what is seen; for the SDW1 state, where no 3rd harmonic is detected, stronger $H\|\mathbf{a}$ polarizability results in the second harmonic δ_{1a}. This behavior is captured in our QOBD model for low applied field, in the helimagnet state. As in the zero-field case, the presence of two modulated states, SDW1 and SDW2, with a jump in q at the transition between them is not found. However, as shown in the Supplemental Material Fig S5 [17], δ_1 becomes dominant over δ_2 on increasing temperature.

For larger fields we expect that a fan state around the field direction becomes energetically favorable. We consider fan states of the form

$$\mathbf{m}_{\text{fan}}(\mathbf{r}) = \begin{pmatrix} m_a \cos\Omega(z) \\ m_b \sin\Omega(z) \end{pmatrix} \tag{2}$$

with $\Omega(z) = \Omega_0 + \Delta \sin(qz)$. Here, Δ is the opening angle of the fan that is centered around the angle Ω_0. We evaluated the free energy density for $H\|\mathbf{b}$ in the FM, deformed helix and fan states following the QOBD approach. By minimizing the free energies we determined the evolution of the magnetic structure as a function of $H\|\mathbf{b}$, shown in the Supplemental Material Fig. S3 [17]. Initially, with increasing field, a deformed helix is favored that undergoes a 1st order transition to a fan state with a larger value of q. On further increasing the field, this fan continuously transforms to a polarized state.

Our experimental results are, therefore, consistent with the QOBD prediction in applied field. Our resistivity study indeed provides evidence for an increase in the DOS. Additionally, inelastic neutron scattering shows enhanced magnetic fluctuations, throughout the SDW3 state. The overall H-T phase diagram for both hard and easy axes is shown in Fig. 4, along with schematics for each magnetic structure.

In conclusion, we have shown PrPtAl may be tuned with field applied along the hard b axis to a singly modulated fan state SDW3, that is well explained by the QOBD theory. At higher temperature, the low field states SDW1 and SDW2 add complexity. We have resolved why the MR initially increases in SDW1 for $H\|\mathbf{a}$. We have also identified qualitatively why SDW1 is more strongly polarizable and therefore preferred in a small field over SDW2, close to T_1. SDW1 and SDW2 are separated by a first order transition and do not necessarily have different symmetry order parameters. Instead they may simply reflect an unstable energy landscape, rather than being intrinsic to the QOBD mechanism.

Field induced modulated order has been seen in 1D and 2D materials, including recently in $Sr_3Ru_2O_7$ [30] at the

boundary between two field polarized states. While QOBD may contribute to stabilizing these modulated states, their low dimensionality means that van Hove singularities and nesting probably dominate the formation mechanism. Noncentrosymmetric $Ca_3Ru_2O_7$ provides another interesting example where polarized helicoid order occurs at high temperatures, between two differently oriented antiferromagnetic states [31,32]. Our results show that modulated state formation may occur more widely when applying a transverse field to a ferromagnet. This could have important implications, for understanding state formation in other materials such as the recently observed field induced superconductivity in UTe_2 [33].

The research data supporting this publication can be accessed at the University of Edinburgh's Datashare repository [34].

We wish to gratefully acknowledge support from the U.K. Engineering and Physical Sciences Research Council Grants No. EP/P013686/1 and No. EP/R013004/1.

*Corresponding author.
chris.oneill@ed.ac.uk

[1] M. Brando, D. Belitz, F. M. Grosche, and T. R. Kirkpatrick, Rev. Mod. Phys. **88**, 025006 (2016).
[2] D. Belitz, T. R. Kirkpatrick, and T. Vojta, Phys. Rev. B **55**, 9452 (1997).
[3] A. V. Chubukov, C. Pépin, and J. Rech, Phys. Rev. Lett. **92**, 147003 (2004).
[4] J. Rech, C. Pépin, and A. V. Chubukov, Phys. Rev. B **74**, 195126 (2006).
[5] C. Pfleiderer and A. D. Huxley, Phys. Rev. Lett. **89**, 147005 (2002).
[6] V. Taufour, D. Aoki, G. Knebel, and J. Flouquet, Phys. Rev. Lett. **105**, 217201 (2010).
[7] M. Uhlarz, C. Pfleiderer, and S. M. Hayden, Phys. Rev. Lett. **93**, 256404 (2004).
[8] G. J. Conduit, A. G. Green, and B. D. Simons, Phys. Rev. Lett. **103**, 207201 (2009).
[9] U. Karahasanovic, F. Krüger, and A. G. Green, Phys. Rev. B **85**, 165111 (2012).
[10] A. G. Green, G. Conduit, and F. Krüger, Annu. Rev. Condens. Matter Phys. **9**, 59 (2018).
[11] G. Abdul-Jabbar, D. A. Sokolov, C. D. O'Neill, C. Stock, D. Wermeille, F. Demmel, F. Krüger, A. G. Green, F. Lévy-Bertrand, B. Grenier *et al.*, Nat. Phys. **11**, 321 (2015).
[12] S. Friedemann, W. J. Duncan, M. Hirschberger, T. W. Bauer, R. Küchler, A. Neubauer, M. Brando, C. Pfleiderer, and F. M. Grosche, Nat. Phys. **14**, 62 (2018).
[13] P. G. Niklowitz, M. Hirschberger, M. Lucas, P. Cermak, A. Schneidewind, E. Faulhaber, J.-M. Mignot, W. J. Duncan, A. Neubauer, C. Pfleiderer *et al.*, Phys. Rev. Lett. **123**, 247203 (2019).
[14] V. Taufour, U. S. Kaluarachchi, R. Khasanov, M. C. Nguyen, Z. Guguchia, P. K. Biswas, P. Bonfà, R. De Renzi, X. Lin, S. K. Kim *et al.*, Phys. Rev. Lett. **117**, 037207 (2016).
[15] U. S. Kaluarachchi, S. L. Bud'ko, P. C. Canfield, and V. Taufour, Nat. Commun. **8**, 546 (2017).
[16] E. Gati, J. M. Wilde, R. Khasanov, L. Xiang, S. Dissanayake, R. Gupta, M. Matsuda, F. Ye, B. Haberl, U. Kaluarachchi *et al.*, Phys. Rev. B **103**, 075111 (2021).
[17] See Supplemental Material at http://link.aps.org/supplemental/10.1103/PhysRevLett.126.197203 for details on sample growth and preparation, experimental setup, the elastic magneticintensity in neutron scattering, magnetoresistance for $H \| a$ axis, and our QOBD theoretical model, which includes Refs. [18–22].
[18] S. Kato, H. Kitazawa, H. Abe, N. Tsujii, and G. Kido, Physica (Amsterdam) **294B-295B**, 217 (2001).
[19] D. Belitz, T. R. Kirkpatrick, and T. Vojta, Phys. Rev. Lett. **82**, 4707 (1999).
[20] J. A. Hertz, Phys. Rev. B **14**, 1165 (1976).
[21] A. J. Millis, Phys. Rev. B **48**, 7183 (1993).
[22] C. J. Pedder, F. Krüger, and A. G. Green, Phys. Rev. B **88**, 165109 (2013).
[23] R. Herz and H. Kronmüller, J. Magn. Magn. Mater. **9**, 273 (1978).
[24] V. I. Zverev, A. M. Tishin, A. S. Chernyshov, Y. Mudryk, K. A. Gschneidner, and V. K. Pecharsky, J. Phys. Condens. Matter **26**, 066001 (2014).
[25] H. Kitazawa, A. Dönni, L. Keller, J. Tang, F. Fauth, and G. Kido, J. Solid State Chem. (France) **140**, 233 (1998).
[26] B. Bleany, Proc. R. Soc. A **276**, 19 (1963).
[27] N. R. Bernhoeft and G. G. Lonzarich, J. Phys. Condens. Matter **7**, 7325 (1995).
[28] C. Zener, Phys. Rev. **96**, 1335 (1954).
[29] J. Jensen and A. R. Mackintosh, *Rare Earth Magnetism, Structures and Excitations, International Series of Monographs on Physics* (Clarendon Press, Oxford, 1991).
[30] C. Lester, S. Ramos, R. S. Perry, T. P. Croft, R. I. Bewley, T. Guidi, P. Manuel, D. D. Khalyavin, E. M. Forgan, and S. M. Hayden, Nat. Mater. **14**, 373 (2015).
[31] D. A. Sokolov, N. Kikugawa, T. Helm, H. Borrmann, U. Burkhardt, R. Cubitt, J. S. White, E. Ressouche, M. Bleuel, K. Kummer *et al.*, Nat. Phys. **15**, 671 (2019).
[32] C. D. Dashwood, L. S. I. Veiga, Q. Faure, J. G. Vale, D. G. Porter, S. P. Collins, P. Manuel, D. D. Khalyavin, F. Orlandi, R. S. Perry *et al.*, Phys. Rev. B **102**, 180410(R) (2020).
[33] S. Ran, I.-L. Liu, Y. S. Eo, D. J. Campbell, P. M. Neves, W. T. Fuhrman, S. R. Saha, C. Eckberg, H. Kim, D. Graf *et al.*, Nat. Phys. **15**, 1250 (2019).
[34] University of Edinburgh's, Datashare repository, https://www.doi.org/10.7488/ds/3024.